Annals of Nuclear Energy 156 (2021) 108206

Contents lists available at ScienceDirect

Annals of Nuclear Energy

journal homepage: www.elsevier.com/locate/anucene

Effects of ion irradiation on Cr, CrN, and TiAlCrN coated Zircaloy-4 for accident tolerant fuel claddings

Ligang Song [a], Bo Huang [a], Jianghua Li [b], Xianfeng Ma [a,*], Min Liu [a], Jishen Jiang [a], Yanying Hu [a]

[a] Sino-French Institute of Nuclear Engineering and Technology, Sun Yat-Sen University, Zhuhai 519082, Guangdong, China
[b] State Key Laboratory of Nonlinear Mechanics (LNM), Institute of Mechanics, Chinese Academy of Sciences, Beijing 100190, China

ARTICLE INFO

Article history:
Received 8 October 2020
Received in revised form 1 February 2021
Accepted 15 February 2021
Available online 6 March 2021

Keywords:
Accident tolerant fuel
Cladding coatings
Zircaloy-4
Au ion irradiation
Grain boundary

ABSTRACT

Heavy ion (6 MeV Au^+) irradiation studies were carried out on three candidate coatings (Cr, CrN, TiAlCrN) and Zircaloy-4 for accident tolerant fuel cladding to investigate the irradiation resistance and microstructure evolution at 400 °C. Transmission Electron Microscopy (TEM) results showed that the irradiation defects were significantly restricted by grain boundaries in the columnar grains compared to equiaxed grains and the high-density boundaries could obviously reduce the formation of voids. Fast Fourier Transformation (FFT) results of high-resolution TEM images showed that Cr and CrN coatings maintained better lattice integrity than those of TiAlCrN coating and Zircaloy-4. ATF coatings showed less irradiation defects than that of Zircaloy-4 substrate. Cr coating exhibited better irradiation resistance than that of TiAlCrN coating in terms of irradiation dislocation loops. CrN coating showed the best irradiation resistance among all samples, due to its compact crystal structure and higher density of grain boundary, which contributed to reduce dislocations and voids.

1. Introduction

Due to its low neutron absorption cross section, good corrosion resistance, microstructural stability and reasonable mechanical properties, Zircaloy-4 has been widely used as nuclear fuel cladding material for light water power reactors (LWR) (Choudhuri et al., 2019; Gaume et al., 2017). The Fukushima-Daiichi accident in 2011, however, drew much attention to the safety and reliability of Zircaloy-4 which would be unavoidable oxidized in high-temperature steam to generate an abundance of heat and hydrogen (Gigax et al., 2019; Skarohlid and Skoda, 2014; Younker and Fratoni, 2016). Accident tolerant fuel (ATF), which is believed to improve the performance at both normal operation and accidental conditions, has attracted worldwide interests of scientists and engineers. Among the different strategy of ATF, the development of anti-oxidation protective coating has been regarded as an effective way to prevent the oxidization of Zircaloy-4. In recent years, several types of promising coatings have been designed and characterized. For example, Cr coatings can exhibit high oxidation resistance when exposed to the steam or air environments under a loss of coolant accidental (LOCA) condition.

However, long-term exposure to irradiation can cause microstructural damage and degradation of cladding material properties such as corrosion resistance, which would limit the performance of ATF coating and Zircaloy-4. There have been some pioneering studies on the irradiation of Cr coatings by neutron, helium ions and heavy ions. Kuprin et al. (Kuprin et al., 2018) reported that the irradiation of chromium coatings causes the isotropic growth of grain size and the swelling up to 0.66% under 1.4 MeV Ar^+ ions irradiation dose of 25 dpa. When Cr coatings were irradiated by He^+ ions irradiation at 400 °C, both the size and density of bubbles increased in the Cr coating with the increase in helium concentration. Helium atoms precipitated preferentially along the Cr grain boundaries to form bubbles and then further gathered to form short bubble microcracks (Huang et al., 2020). Moreover, heavy ions such as Au^+ irradiation causes more dislocation loops at 400 °C and the evolution of irradiation defects is delayed in thinner Cr coatings (Jiang et al., 2019). The nanostructured nitrides perform high irradiation tolerance. Some other coatings such as CrN can maintain the continuous and columnar structure after the 600 keV Kr^{3+} ion irradiation with a fluence of 1×10^{17} Kr^{3+}/cm^2 (Wu et al., 2019). Besides, the CrN coating largely remained intact apart from several local spots where the coating had cracked or disappeared in Boiling and Pressurized Water Reactor (PWR) in-pile experiments, in which the TiAlN and AlCrN coatings both disappeared after the irradiation (Van

* Corresponding author at: Sino-French Institute of Nuclear Engineering and Technology, Sun Yat-Sen University, Zhuhai 519082, Guangdong, China (X. Ma).
E-mail address: maxf6@mail.sysu.edu.cn (X. Ma).

https://doi.org/10.1016/j.anucene.2021.108206
0306-4549/

Nieuwenhove et al., 2018). Recently, TiAlCrN coatings have performed excellent mechanical properties and oxidation resistance properties (Ma et al., 2019). However, the irradiation resistance difference between typical ATF candidate coatings and Zircaloy-4 has been rarely reported. It is an important concern in the selection and evaluation of ATF coating technology.

In this work, Cr, CrN and TiAlCrN coatings were prepared on Zircaloy-4 using multi-arc ion plating technique. Heavy ion irradiation experiments were carried out to induce irradiation damage in the three ATF coatings and the Zircaloy-4 substrate. To investigate the irradiated microstructure evolution at different depths, all irradiated samples were subjected to the focused ion beam (FIB) processing to obtain TEM foils. Cross-sectional transmission electron microscopy (TEM) characterization and analysis were conducted to reveal the effects of microstructure in different coatings on the formation and evolution of irradiation defects.

2. Materials and experimental procedure

2.1. Materials fabrication

The Zircaloy-4 used in this study has a chemical composition as given in Table 1. The as-received Zircaloy-4 sheet was machined into a 25 mm × 15 mm × 2 mm sheet using electrical wire cutting. The samples were subjected to a subsequent annealing at 650 °C for 1 h in a vacuum tube to remove residual stress. The sample surfaces were grinded by 400, 600, 1000, and 1500 grit SiC papers and polishing from 3 μm down to 1 μm.

The Cr, CrN, and TiAlCrN coatings were deposited on the Zircaloy-4 substrate by the multi-arc ion plating technique. The samples were hung on the holder and rotated at a constant speed to obtain homogenously deposited coating. Before deposition, sputter cleaning was performed on the samples to remove the oxide from the Zircaloy-4 sample surface. The Cr coatings were deposited using two high-purity (99.999%) Cr cathodes under a negative substrate bias voltage of 75 V, an arc current of 100 A, a pressure of 2.7 Pa, a deposition temperature of 340 °C, and a deposition time of 6 h. To prepare the CrN coating, a Cr-bond coating was firstly deposited on the Zircaloy-4 substrate to enhance the interfacial strength. During the deposition of the CrN layer, the nitrogen filling pressure was maintained at 1.3–1.5 Pa. The temperature of the Zircaloy-4 substrate was kept at 400 °C during deposition.

To prepare the TiAlCrN coatings, a Cr bond coating approximately 100 nm thick was first deposited on the Zircaloy-4 substrate under an argon atmosphere at a pressure of 0.3 Pa to enhance the interfacial adhesion. Two high-purity (99.999%) Cr cathodes and two TiAl (25–75 at.% Al) cathodes were used for the deposition of TiAlCrN layers under a negative substrate bias voltage of 70 V, an arc current of 100 A, and a pressure of 0.3 Pa. The temperature of the substrate was kept at 400 °C during deposition as well.

2.2. Ion irradiation

For heavy ion irradiation tests, 6 MeV Au^+ ions were used to irradiate samples at 400 °C with a dose of $1.45 \times 10^{15} ions/cm^2$. The irradiation experiments were performed at 2 × 3 MV electrostatic tandem accelerator at the Institute of Nuclear Science and Technology, Sichuan University. The irradiation damage of 6 MeV Au ions and the depth distribution of Au atoms were simulated by using SRIM-2013 software with the "Quick calculation of damage" mode (Ziegler et al., 2010). A displacement energy of 40 eV is considered for Zr, Cr, Al and Ti elements, while 25 eV is considered for N element. Fig. 1 shows the results of DPA versus irradiation depth. The depth of damage peak and the maximum depth of damage area in four materials were given in parentheses. It is noted that the distribution of irradiation damage in CrN is similar to that in TiAlCrN. The maximum depth of damage area in Zr is the same as that in CrN.

In addition, the thickness of the Cr, CrN, and TiCrAlN coating in this study are around 10 μm. In present study, there is little effect of thickness on the irradiation behavior of the coatings, as the irradiated depth was less than 1.5 μm in all studied coatings. For a thin coating, the coating thickness might affect the irradiation behavior of Cr coating. For instance, Jiang et al (Jiang et al., 2019) studied the Cr coating interface irradiated by Au ions to a dose of 10, 25 and 50 dpa and found that the number density of loops decreased while the size increased with increasing thickness from 5 μm to 12 μm. For this study, the irradiation damage of the Cr, CrN, and TiCrAlN coating (~10 μm) are all below 10 dpa, for which the number density of defects was lower than that of high dose (Jiang et al., 2019).

2.3. TEM samples fabrication and analysis

The TEM samples were fabricated by focused ion beam (FIB) lift-out technique (see Fig. 2) with a FEI Quanta 3D FEG dual beam scanning electron microscopy (SEM). TEM analysis was carried out on an FEI Talos 200X TEM microscope to study the damage accumulation after irradiation. In Fig. 2, the middle areas of the foils were further thinning and then imaged at high-resolution TEM (HRTEM) mode. The thickness of Zircaloy-4, Cr, CrN and TiAlCrN foils are 101.2 nm, 73.38 nm, 91.73 nm and 94.43 nm, respectively. General image processing, including FFT of images and inverse FFT, was carried out using the Digital Micrograph software. Transmis-

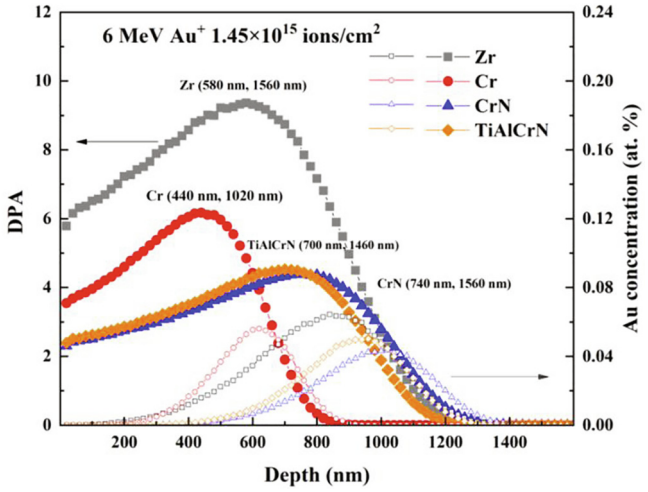

Fig. 1. SRIM results for damage production in Zr, Cr, CrN, TiAlCrN irradiated by 6 MeV Au ions with a fluence of 1.45×10^{15} ions/cm^2.

Table 1
Chemical composition of the Zircaloy-4 in this study.

	Sn	Fe	Cr	N	O	H	Zr
wt%	1.2–1.7	0.18–0.24	0.07–0.13	0.008	0.16	0.01	Bal.

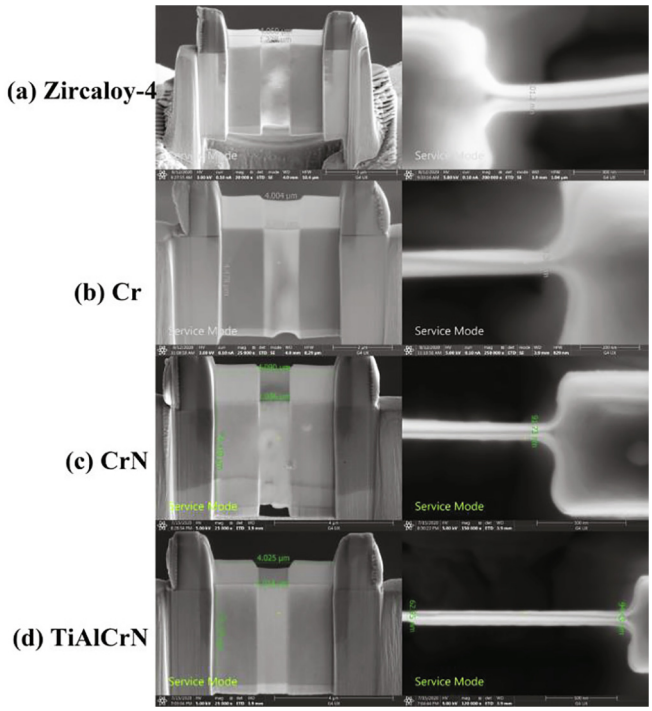

Fig. 2. The TEM lift-outs morphology and thickness of Cr, CrN, TiAlCrN coatings and Zircaloy-4. The middle area of every sample were further thinning for HRTEM modes.

sion Kikuchi diffraction (TKD), or called t-EBSD analysis, was also carried out under the SEM. The spatial resolution of the TKD technique can be estimated as being in the range of 5–10 nm (Trimby, 2012). The TEM foils were mounted using a micro-clamp SEM substage that was fixed to a standard 70° tilted EBSD sample holder. The SEM stage was then tilted towards the EBSD detector by 20°, resulting in the TEM foils being oriented horizontally. The EBSD detector was fully inserted into its standard operating position with a data acquisition speed at 22.25 Hz. The SEM was operated with an accelerating voltage valued 25 kV.

3. Result and discussion

Fig. 3 shows the FIB sample morphology and corresponding EBSD IPF map of Cr, CrN, TiAlCrN coatings and Zircaloy-4 after Au ions irradiation. It is known that original Zircaloy-4 comprises the alpha phase with a hexagonal close packed crystal structure (He et al., 2019). The original CrN coating is highly uniform and compact and the top planes of the columnar crystal on the surface stacked on each other, forming a typical poly-crystalline microstructure (Meng et al., 2019). The as-deposited TiAlCrN coating shows diffraction peaks assigned to an fcc NaCl-type structure with a [200] preferential orientation. The Ti, Al, and Cr elements might occupy lattice positions at random in the single fcc NaCl-type structure (Ma et al., 2019). In Fig. 3(a), the grain orientation map of Zircaloy-4 showed two major grain orientations with discontinuous black areas. It indicates that the hexagonal crystal structure of Zircaloy-4 was affected by heavy ion irradiation and may not be close packed. However, the grain boundary of Zircaloy-4 is still distinguishable, with irradiation defects widely distributed in the grains. In Fig. 3(b), the grains of Cr coatings showed columnar structure with two major orientations. The average width of Cr grains is about 1.2 μm. The columnar grains are through the coating thickness. However, the coating thickness of Cr coating is beyond the depth of foils, which make the whole columnar grains not entirely displayed. The Cr coating maintained complete crystal structure with clear grain boundary after irradiation. The grain boundary of Cr coating extends from the interface to the sample surface. For the CrN coating, there are still a few large grains. The small grains may be difficult to detect by EBSD, leading to the rest region dark as shown in Fig. 3(c). In Fig. 3(d), the TiAlCrN coating shows no obvious crystal structure which was probably influenced by the Ti, Al, and Cr elements in the crystal structure of as-deposited TiAlCrN coating.

3.1. Microstructure of Zircaloy-4 after irradiation

Fig. 4 shows the irradiated microstructure of Zircaloy-4 under detailed TEM examination. In Fig. 4(a), the dash white line and solid line represent the peak damage position and the maximum irradiation depth, respectively. Hereafter the white dotted and solid lines have the same meaning.

Zircaloy-4 irradiated by Au ions showed disordered structure morphology, as shown in Fig. 4(a). To investigate the details of irradiation area, two different regions (from surface to damage peak position and from damage peak position to maximum irradiation depth) and the corresponding magnified images were shown in Fig. 4. In Fig. 4(d), many black dots accumulated in the area near the surface. Compared to the top left area of Fig. 4(a), the microstructure of Zircaloy-4 close to the surface was disordered. The ion irradiation could cause the irradiated surface of Zircaloy-4 to become amorphous (Wan et al., 2006). In the deep layer, the number of black dots decreased and dislocation loops or dislocations were observed in Fig. 4(c) and Fig. 4(e). With increasing irradiation damage, the black dots would grow into dislocations. M. Gaume et al. (Gaume et al., 2017) reported that after 600 keV Zr ion irradiation, when increasing the irradiation temperature, the loop number density decreased and the mean loop diameter increased. No evident effect of damage dose on the final microstructure was observed. Moreover, M. Topping et al. found (Topping et al., 2019) that Nb-containing Zr-alloy showed small variation of loop size and line density when irradiated by proton with a damage level of 2 dpa at 280 °C, 350 °C and 450 °C. The < a > -dislocation loops were always very small and numerous. In addition, the formation of < c>- type dislocation loops was observed after irradiation at 80 °C and 200 °C, but not at 450 °C and 550 °C (Yu et al., 2017).

3.2. Microstructure of Cr coating after irradiation

Fig. 5 shows the microstructure features of Cr coating after ion irradiation by TEM examination. The typical grain boundary in Cr coating marked by red arrow in Fig. 5(a) is long and perpendicular to the surface. The grain boundaries can usually act as sinks for microscopic defects of all types. Although grain boundaries play an important role in absorbing irradiation induced point defects (El-Atwani et al., 2018), the voids still exist in the internal of large-size grains as shown in the enlarged image of Fig. 5(f). The production of voids depends on the accumulation of point defects like vacancies. It is evident that there were little voids formed at the area near the grain boundary, which called the denuded zones. And with increasing distance away from the grain boundary, the density of voids increased rapidly and the average size of voids was slightly decreased. The increased nucleation rate of voids would reduce the growth of voids.

Kuprin et al. (Kuprin et al., 2018) reported that increasing the Ar^+ ion irradiation dose from 5 dpa to 25 dpa would increase the mean size of voids from 1.5 to 4 nm in Cr coating at 400 °C (T/Tm = 0.31). It is consistent with the present study that the void size in irradiated Cr coating was quite small. The Au + ion irradiation dose in Cr coating at 400 °C is ~6 dpa, less higher than 5 dpa. There-

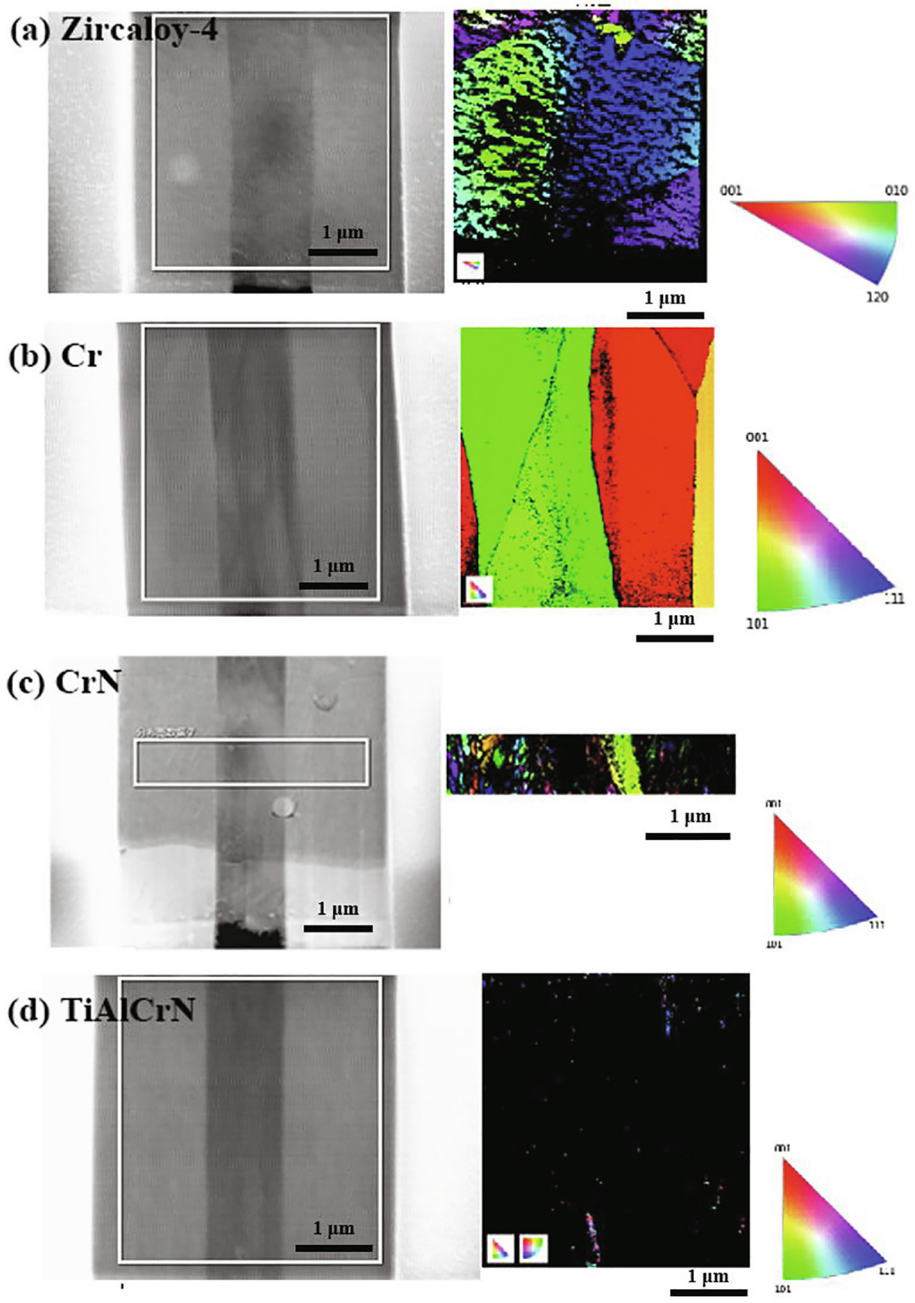

Fig. 3. Morphology and crystal orientation map of Cr, CrN, TiAlCrN coatings and Zircaloy-4 after Au ions irradiation.

fore, the mean size of voids may be close to 1.5 nm. The voids were too small to affect the grain structure. Therefore, Cr coatings maintained almost complete crystal structure after Ar^+ ion irradiation as shown in Fig. 3(b), indicating that Cr coating has a good irradiation resistance.

3.3. Microstructure of CrN coating after irradiation

Fig. 6 shows the irradiated microstructure of CrN coating by TEM observation. In Fig. 6(a), the morphology of CrN coating shows grain boundaries approximately perpendicular to the surface. Some artificial stripes along vertical were observed in Fig. 6b, which were due to the sample preparation by FIB. The grain distribution feature of CrN coating was similar to that of Cr coating except for the density of grain boundary. Moreover, voids were not noticed in the CrN coating, in contract to that of Cr coating. The production of voids depends on accumulation of point defects like vacancies. The grain boundaries in materials can act as potent sinks for point defects. For large grains, many mobile defects cluster in the grain interior, annihilate at interior sinks such as dislocations, or undergo mutual recombination of vacancy-SIA pairs. As the grain size decreases to the nanoscale, it approaches the mean free path for mutual recombination. Moreover, interior sinks such as dislocations become scarcer. Consequently, mobile defects have a much higher likelihood of reaching grain boundaries before recombination or annihilation in the grain interior (Zhang et al., 2012). The sink strength of grain boundary is not only determined by the long-range point defect diffusion but also the short-range point defect absorption by the dynamic climbing of grain boundary dislocations (Liu et al., 2019). The mobility of defects varies signif-

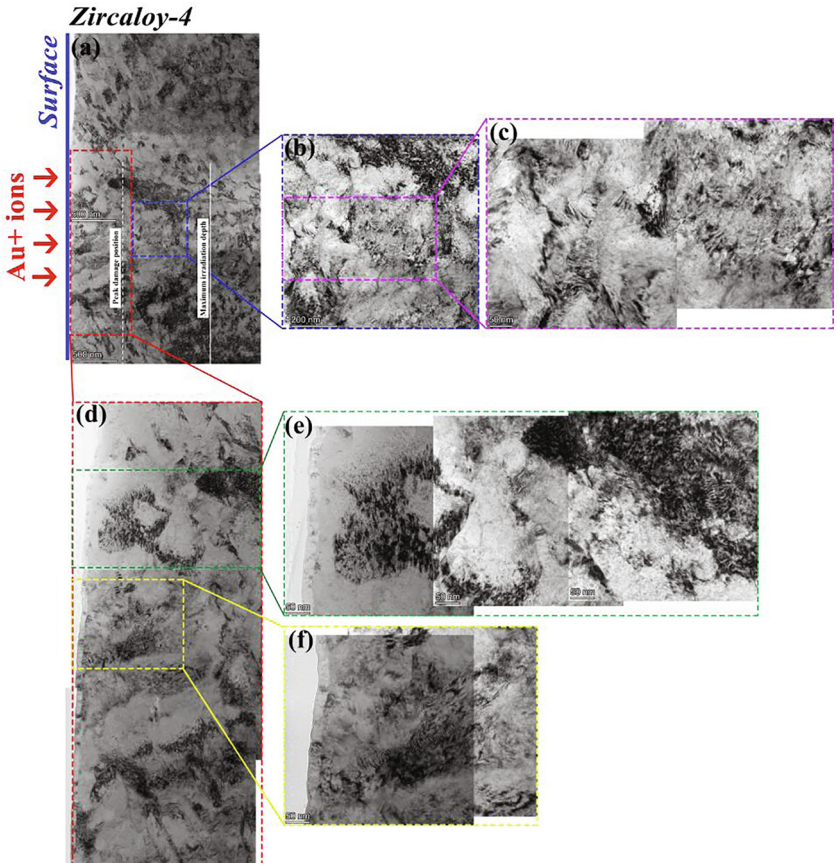

Fig. 4. The whole area of TEM image and corresponding magnification image for Zircaloy-4. The same colored outlines represent the same area.

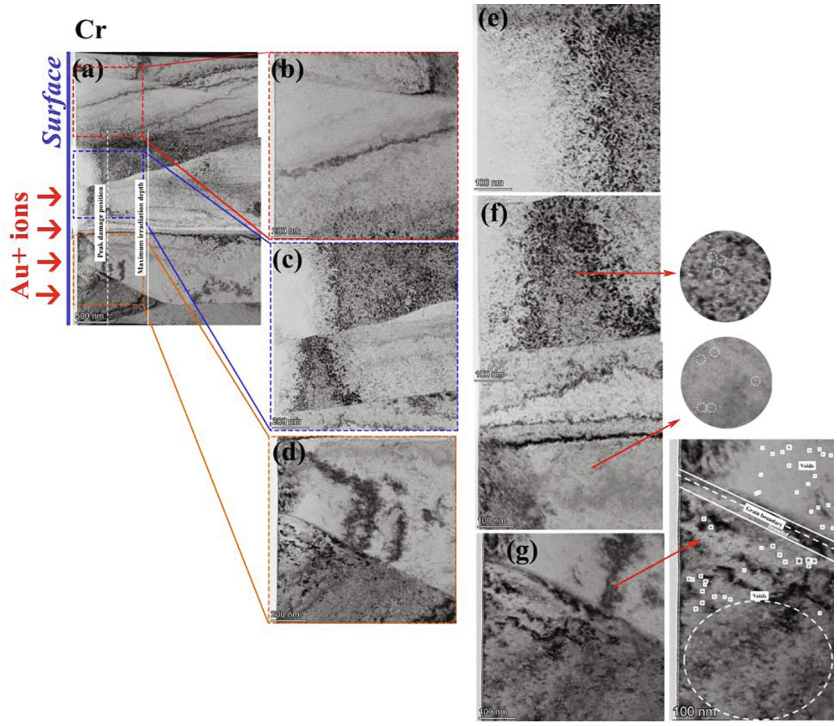

Fig. 5. The whole area of TEM image and corresponding magnification image for Cr coating. The same colored outlines represent the same area.

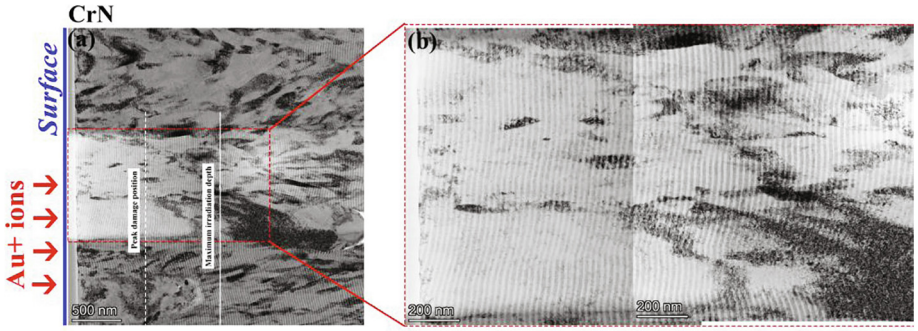

Fig. 6. The whole area of TEM image and corresponding magnification image for CrN coating. The same colored outlines represent the same area.

icantly with boundary structure and cluster size. Larger clusters exhibit reduced mobility. The defect mobility at boundaries can be slower than in the bulk (Uberuaga et al., 2015).

It is indicated that the higher density of grain boundary in CrN coating must be beneficial to restrict the nucleation and growth of voids. The existence of high-density grain boundary act as sinks for defects like vacancies. When the vacancies migrate to the area near a grain boundary, they are easily absorbed by the grain boundary. The production of voids depends on accumulation of point defects like vacancies. When the diffusion and aggregation of vacancies are restricted by high-density grain boundary, the voids are not easily produced. The voids in CrN coating are hard to spot and the number of voids would be much less than that in Cr coating. Similar effects were also reported in CrN coating by He^+ ion irradiation at 500 °C by Tang et al. Besides, small He bubbles with low bubble densities were observed in the irradiated nanochannel CrN coating (Tang et al., 2018). However, the sink strength and efficiency of grain boundaries would change as more defects (either vacancies or SIAs) are absorbed in the boundary region. The atomic structure might become instable.

3.4. Microstructure of TiAlCrN coating after irradiation

In Fig. 7, the morphology of TiAlCrN coating shows finer microstructure features than that of CrN coating. As mentioned in the EBSD results shown in Fig. 3, there were much more small grains in TiAlCrN coating than the other coatings. Similar to CrN coating, voids were rarely observed in the TiAlCrN coating which has denser grain boundaries. It indicates that a high density of grain boundary can significantly affect the existence of voids. The defects were evenly distributed in the irradiation area, partially due to the distribution of grain boundaries.

3.5. Comparison of irradiated microstructures in Zircaloy-4, Cr, CrN and TiAlCrN coatings

Fig. 8 shows the bright field (BF) TEM images of the irradiated microstructures of Zircaloy-4 in comparison to the three ATF coatings. Fig. 8(a) shows the disordered microstructure morphology of Zircaloy-4. On the left side of the peak damage position (dashed line), there are evidently some linear interfaces between the shadow areas and bright areas which gradually become wavy lines with increasing depth. Fig. 9(b) shows typical structure of column crystal in Cr coatings, consistent with EBSD results in Fig. 3. The linear interface exhibited long and straight along the direction from surface to matrix with the existence of large columnar crystal. Although similar interface microstructures were observed in CrN coating (Fig. 9(c)) and TiAlCrN coating (Fig. 9(d)), the distributions of shadow areas in the two coatings were quite different. From the DF-TEM image, the three coatings have similar linear type interface except for different sizes, which is consistent with the results in BF-TEM images. With increasing density of columnar grain boundaries, the bright areas gradually decreased. As mentioned above, grain boundaries with specific structures can restrict the distribution of defects. However, in the DF-TEM image of Zircaloy-4, there were only bright areas of distortion in the equiaxed crystal.

Small grain sizes and large volume fractions of grain boundaries or interfaces could absorb and annihilate the mobile defects pro-

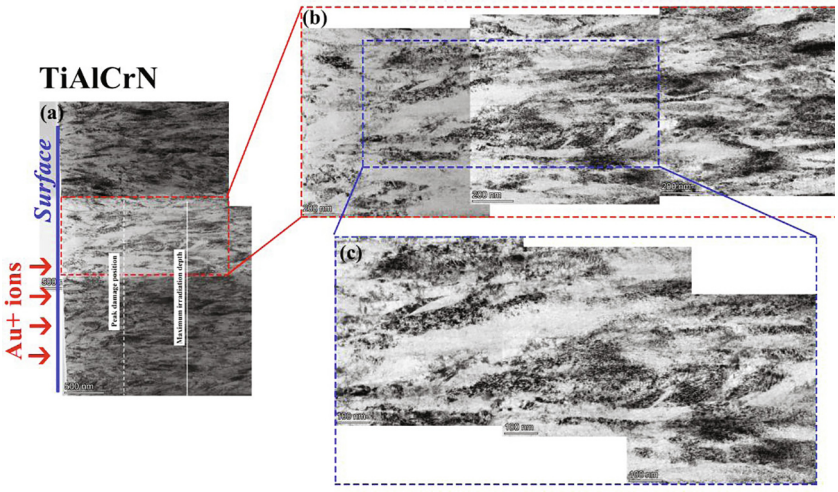

Fig. 7. The whole area of TEM image and corresponding magnification image for TiAlCrN coating. The same colored outlines represent the same area.

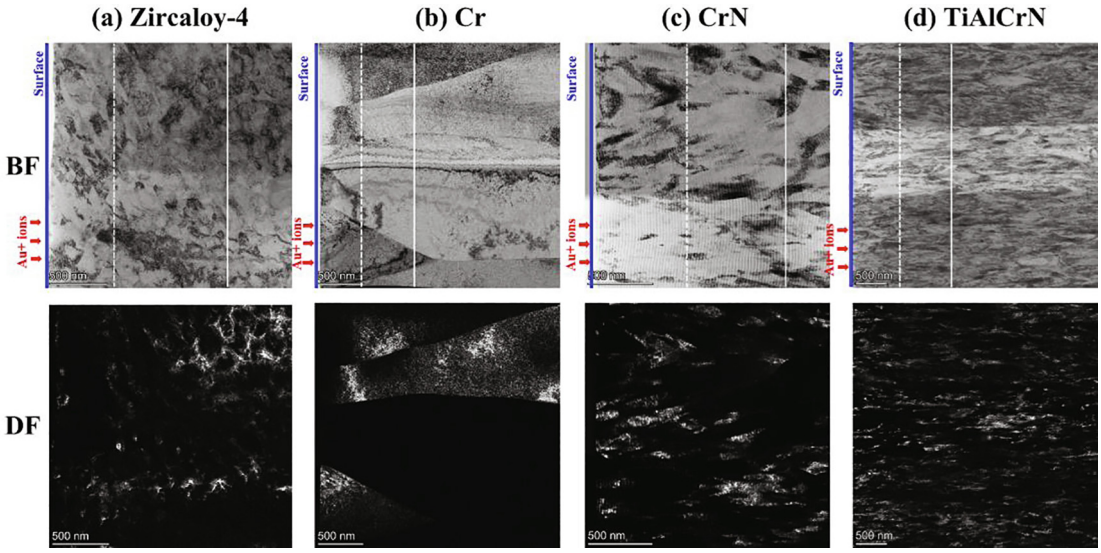

Fig. 8. Bright field (up) and corresponding dark field (down) TEM images for (a) Zircaloy-4, (b) Cr, (c) CrN, (d) TiAlCrN after irradiation. The ions incident direction is consistently from the left to the right. The left edge corresponds to the sample surface in all images of (a)-(d). The dashed and solid lines represent the peak damage position and the maximum irradiation position, respectively.

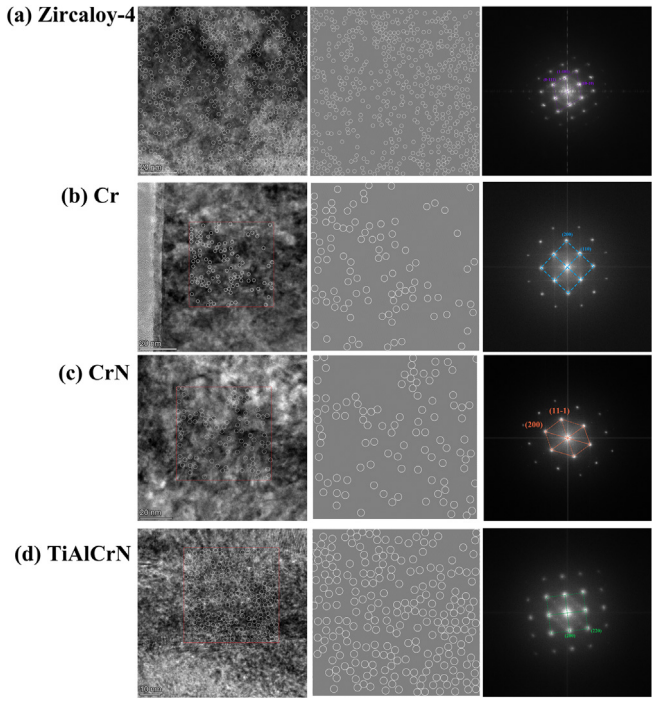

Fig. 9. The HRTEM image (left column) for (a) Zircaloy-4, (b) Cr, (c) CrN, (d) TiAlCrN and corresponding FFT image (right column) in irradiation area. The center column images of each sample was made by inversing FFT image with only a pair of diffraction spots for investigating dislocations. When the dislocation exists, it is marked with a white circle, which is also shown in HRTEM image (left column).

duced by irradiation (El-Atwani et al., 2018). In order to characterize the internal microstructures of grains in the irradiation area, HRTEM and corresponding FFT images were used to probe the disloactions and the substructure, as is shown in Fig. 9. FFT images show that Zircaloy-4 substrate has a hexagonal close-packed (HCP) crystal structure. Cr coating shows body-centered cubic (BCC) crystal structure, whereas CrN and TiAlCrN coatings have face-centered cubic (FCC) crystal structure. Different crystal structure would make contribution to the different features after irradiation. Eldrup M. M. et al. (Eldrup and Singh, 2001) found that, by neutron irradiation, void nucleating took place only at irradiation temperatures above ~200 °C in copper (FCC). On the other hand, voids were formed in the whole temperature range (50–350 °C). In addition, a high density of smaller vacancy agglomerates (micro-voids) was found to nucleate at the lower irradiation temperatures. Furthermore, Khara G.S. et al. (Khara et al., 2017) found the high thermal conductivity and relatively low electron–phonon coupling of fcc metals render them relatively insensitive to damage, in spite of their relatively low melting temperatures. The strong electron–phonon coupling of the bcc metals (Fe and W) was primarily responsible for the sensitivity of these metals to damage. In case of HCP metal Zr, Hashimoto N. et al. (Hashimoto et al., 2004) found that the number density of small loops (about 2 nm in size) in Zr (HCP) was much lower ($\sim 7 \times 10^{22}$ m^{-3}) than that of Cu (FCC) and V (BCC) when all metals were irradiated by neutron at low temperature. In addition, point defect production is usually different between cubic systems (FCC/BCC) and HCP systems. In the FCC/BCC system, point defects, including self-interstitials (SIAs) and vacancies, diffuse isotropically. However, due to the crystallographic anisotropy of HCP structure, the diffusion of point defects often occurs. The evolution of irradiation-induced defects has a strong correlation with c/a ratio and impurities (Li et al., 2018). Hence the point defect production is more complex in Zircaloy-4 (HCP) than in Cr (BCC) or CrN and TiAlCrN (FCC).

According to the diffraction pattern, Cr, CrN, TiAlCrN coatings and Zircaloy-4 in the selective irradiation area showed single crystalline structure. In Fig. 9, dislocation loops were marked by white circles. By calculation, the number density of white circles in Zircaloy-4, Cr, CrN, TiAlCrN are $6.754 \times 10^{23}/m^3$, $6.568 \times 10^{23}/m^3$, $3.29 \times 10^{23}/m^3$, $1.21 \times 10^{24}/m^3$, respectively. As mentioned above, although the grain boundaries can act sinks of irradiation defects, the number density of dislocations in grains did not decrease with increasing density of grain boundary for CrN and TiAlCrN coatings. Although the TiAlCrN coating had a smaller grain size and higher grain boundary density, the number density of dislocations was larger than that of CrN coating. Moreover, the grain boundaries were also characterized by excess energy which could provide a shift in the total free energy that

would lead to the amorphization process of materials during irradiation (Barr et al., 2018; Shi et al., 2015). Therefore, the diffraction spot of TiAlCrN was not so sharp. It is interesting to note that the CrN coating show a better radiation resistance than TiAlCrN coating. Not only the dislocation density of CrN was lower than that of TiAlCrN, but also the void did not appear in bulk and the crystal structure remained intact. Hence, it is indicated that appropriate grain boundary density would make better contribution to restrict the production of voids and dislocations and avoid the increasing energy of material system induced by high density of grain boundaries.

In the present study, Cr coating showed a large column grains with BCC structure on a Zircaloy-4 substrate. The mobile defects were easily restricted in the grain interior, annihilated at interior sinks such as dislocations. But the defects like vacancies could also form cluster in the grain interior or grain boundary. CrN coating with FCC structure showed denser grain boundaries than Cr coating, which could make the defects well-distributed. Also, the FCC structure seemed to be less sensitive to irradiation damage. But the high density grain boundaries would increase the energy of material system. The results indicated that CrN coating exhibited better irradiation resistance than Cr coating herein.

4. Conclusion

In summary, the effects of heavy ion irradiation on the microstructures of Cr, CrN, TiAlCrN coatings and Zircaloy-4 have been investigated by TEM analysis. The following conclusions have been obtained:

(1) The ATF coatings exhibited better irradiation resistance than that of Zircaloy-4, indicated by less irradiation defects. The number density of dislocation loops in Zircaloy-4, Cr, CrN, TiAlCrN were measured to be $6.754 \times 10^{23}/m^3$, $6.568 \times 10^{23}/m^3$, $3.29 \times 10^{23}/m^3$, $1.21 \times 10^{24}/m^3$, respectively.
(2) TEM results showed that the irradiation defects were significantly restricted by grain boundaries in the columnar grains compared to equiaxed grains and the high-density boundaries could obviously reduce the formation of voids. Fast Fourier Transformation results of HRTEM images showed that Cr and CrN coatings maintained better lattice integrity than those of TiAlCrN coating and Zircaloy-4.
(3) Cr coating exhibited better irradiation resistance than TiAlCrN coating in terms of irradiation dislocation loops. High density of grain boundaries in CrN and TiAlCrN coatings could significantly reduce the number of voids and voids were rarely observed in these two coatings. The number density of irradiation defects was slightly larger in TiAlCrN coating than that in CrN coating.
(4) CrN coating showed the best irradiation resistance among all samples, due to its compact crystal structure and higher density of grain boundary, which contributed to reduce dislocations and voids.

CRediT authorship contribution statement

Ligang Song: Formal analysis, Investigation, Writing - original draft, Data curation. **Bo Huang:** Writing - review & editing, Investigation. **Jianghua Li:** Methodology, Conceptualization, Data curation. **Xianfeng Ma:** Conceptualization, Resources, Supervision, Funding acquisition, Project administration. **Min Liu:** Writing - review & editing, Investigation. **Jishen Jiang:** Writing - review & editing, Investigation, Funding acquisition. **Yanying Hu:** Writing - review & editing, Investigation.

Declaration of Competing Interest

The authors declare that they have no known competing financial interests or personal relationships that could have appeared to influence the work reported in this paper.

Acknowledgement

This project is supported by the National Science Foundation of China (No. U2032143, 11902370, 52005523), Guangdong Major Project of Basic and Applied Basic Research (2019B030302011), International Sci & Tech Cooperation Program of GuangDong Province (2019A050510022), Key-Area Research and Development Program of GuangDong Province (2019B010943001, 2017B020235001), China Postdoctoral Science Foundation (2019 M653173 and 2019TQ0374), Guangdong Education Department Fund (2016KQNCX005), and Fundamental Research Funds for the Central Universities (19lgpy304).

References

Barr, C.M., N. Li, B.L. Boyce, et al. (2018) Examining the influence of grain size on radiation tolerance in the nanocrystalline regime.Applied Physics Letters, 112:
Choudhuri, G., Mishra, P., Basu, S., et al., 2019. Effect of ion and neutron irradiation on oxide of PHWR fuel tube material. J. Nucl. Mater. 514, 12–27.
El-Atwani, O., Esquivel, E., Efe, M., et al., 2018. Loop and void damage during heavy ion irradiation on nanocrystalline and coarse grained tungsten: microstructure, effect of dpa rate, temperature, and grain size. Acta Materialia 149, 206–219.
El-Atwani, O., Martinez, E., Esquivel, E., et al., 2018. Does sink efficiency unequivocally characterize how grain boundaries impact radiation damage?. Phys. Rev. Mater. 2.
Eldrup, M., B.N. Singh. (2001) Void nucleation in fcc and bcc metals: A comparison of neutron irradiated copper and iron. Positron Annihilation - Icpa-12, 363-3:79-81.
Gaume, M., Onimus, F., Dupuy, L., et al., 2017. Microstructure evolution of recrystallized Zircaloy-4 under charged particles irradiation. J. Nucl. Mater. 495, 516–528.
Gigax, J.G., Kennas, M., Kim, H., et al., 2019. Radiation response of Ti2AlC MAX phase coated Zircaloy-4 for accident tolerant fuel cladding. J. Nucl. Mater. 523, 26–32.
Hashimoto, N., Byun, T.S., Farrell, K., et al., 2004. Deformation microstructure of neutron-irradiated pure polycrystalline metals. J. Nucl. Mater. 329, 947–952.
He, X.J., Tian, Z.H., Shi, B.H., et al., 2019. Effect of gas pressure and bias potential on oxidation resistance of Cr coatings.Annals of. Nucl. Energy 132, 243–248.
Huang, M.J., Li, Y.P., Ran, G., et al., 2020. Cr-coated Zr-4 alloy prepared by electroplating and its in situ He+ irradiation behavior. J. Nucl. Mater. 538.
Jiang, L., Xiu, P.Y., Yan, Y., et al., 2019. Effects of ion irradiation on chromium coatings of various thicknesses on a zirconium alloy. J. Nucl. Mater. 526.
Khara, G.S., S.T. Murphy, D.M. Duffy. (2017) Dislocation loop formation by swift heavy ion irradiation of metals. Journal of Physics-Condensed Matter, 29:
Kuprin, A.S., Belous, V.A., Voyevodin, V.N., et al., 2018. Irradiation resistance of vacuum arc chromium coatings for zirconium alloy fuel claddings. J. Nucl. Mater. 510, 163–167.
Li, J., Chen, Y., Wang, H., et al., 2018. In situ study on enhanced heavy ion irradiation tolerance of porous Mg. Scripta Materialia 144, 13–17.
Liu, P.C., Zheng, S.L., Chen, K.G., et al., 2019. Point defect sink strength of low-angle tilt grain boundaries: a phase field dislocation climb model. Int. J. Plast. 119, 188–199.
Ma, X.F., Wu, Y.W., Tan, J., et al., 2019. Evaluation of corrosion and oxidation behaviors of TiAlCrN coatings for nuclear fuel cladding. Surf. Coat. Technol. 358, 521–530.
Meng, C.Y., Yang, L., Wu, Y.W., et al., 2019. Study of the oxidation behavior of CrN coating on Zr alloy in air. J. Nucl. Mater. 515, 354–369.
Shi, J.Y., L. Peng, M.Y. Ye, et al., DEFECT EFFECTS ON GRAIN BOUNDARY STRENGTH IN FE: A MOLECULAR DYNAMICS SIMULATION. 2015 Ieee 26th Symposium on Fusion Engineering. 2015, New York: Ieee.
Skarohlid, J., R. Skoda. (2014) Polycrystalline Diamond Films as Protection of Zircaloy Fuel Cladding.Proceedings of the 22nd International Conference on Nuclear Engineering - 2014, Vol 1,
Tang, J., Hong, M.Q., Wang, Y.Q., et al., 2018. Microstructural evolution of nanochannel CrN films under ion irradiation at elevated temperature and post-irradiation annealing. J. Nucl. Mater. 500, 242–251.
Topping, M., Harte, A., Ungar, T., et al., 2019. The effect of irradiation temperature on damage structures in proton-irradiated zirconium alloys. J. Nucl. Mater. 514, 358–367.
Trimby, P.W., 2012. Orientation mapping of nanostructured materials using transmission Kikuchi diffraction in the scanning electron microscope. Ultramicroscopy 120, 16–24.
Uberuaga, B.P., L.J. Vernon, E. Martinez, et al. (2015) The relationship between grain boundary structure, defect mobility, and grain boundary sink efficiency. Scientific Reports, 5.

Van Nieuwenhove, R., V. Andersson, J. Balak, et al. (2018) In-Pile Testing of CrN, TiAlN, and AlCrN Coatings on Zircaloy Cladding in the Halden Reactor. Zirconium in the Nuclear Industry: 18th International Symposium, 1597:965-982.

Wan, Q.A., Bai, X.D., Zhang, X.Y., 2006. Impact of high dose krypton ion irradiation on corrosion behavior of laser beam welded zircaloy. Mater. Res. Bull. 41, 387–395.

Wu, Z., Wu, Y.M., Wang, Q.M., 2019. A comparative investigation on structure evolution of ZrN and CrN coatings against ion irradiation. Heliyon 5.

Younker, I., Fratoni, M., 2016. Neutronic evaluation of coating and cladding materials for accident tolerant fuels. Progr. Nucl. Energy 88, 10–18.

Yu, H.B., Liang, J.L., Yao, Z.W., et al., 2017. Effect of heavy ion irradiation on thermodynamically equilibrium Zr-Excel alloy. J. Nucl. Mater. 488, 33–45.

Zhang, Y.F., Huang, H.C., Millett, P.C., et al., 2012. Atomistic study of grain boundary sink strength under prolonged electron irradiation. J. Nucl. Mater. 422, 69–76.

Ziegler, J.F., M.D. Ziegler, J.P. Biersack. (2010) SRIM - The stopping and range of ions in matter (2010).Nuclear Instruments & Methods in Physics Research Section B-Beam Interactions with Materials and Atoms, 268:1818-1823.